IEEE Access
Multidisciplinary | Rapid Review | Open Access Journal

Received January 23, 2018, accepted February 23, 2018, date of publication March 2, 2018, date of current version April 4, 2018.

Digital Object Identifier 10.1109/ACCESS.2018.2811387

Uplink Area Spectral Efficiency Analysis for Multichannel Heterogeneous Cellular Networks With Interference Coordination

HONG WANG[1,2], SHU-HUNG LEUNG[3], AND RONGFANG SONG[1]

[1]School of Communication and Information Engineering, Nanjing University of Posts and Telecommunications, Nanjing 210003, China
[2]National Mobile Communications Research Laboratory, Southeast University, Nanjing 210096, China
[3]State Key Laboratory of Millimeter Waves, Department of Electronic Engineering, City University of Hong Kong, Hong Kong

Corresponding author: Hong Wang (wanghong@njupt.edu.cn)

This work was supported in part by the Natural Science Foundation of Jiangsu Province under Grant BK20170910, in part by the Open Research Foundation of the National Mobile Communications Research Laboratory, Southeast University, under Grant 2018D09, in part by NSF of Jiangsu Higher Education Institutions under Grant 16KJB510035, in part by the Research Grants Council of the Hong Kong Special Administrative Region, China, under Grant CityU-11272516, and in part by the Theme-Based Research under Grant T42-103/16-N.

ABSTRACT The deployment of small cells (SCs) in heterogeneous cellular networks (HCNs) has been shown to be a promising approach to increase the system capacities of wireless communications. However, the bandwidth sharing and densification of the SCs cause co-tier and cross-tier interferences that limit the system spectral efficiency. In this paper, a framework of an uplink area spectral efficiency (ASE) analysis for multichannel HCNs using a proposed biased cell association scheme with coordinated subchannel allocation and channel inversion power control for mitigating the interferences is developed. The coordinated subchannel allocation is proposed to alleviate the severe cross-tier interference caused by macrocell users around the edges of the SCs. By incorporating the coordinated subchannel allocation into the biased cell association scheme with a bias factor, the proposed scheme is able to design the bias factor to reshape the coverage areas of the SCs providing an effective tradeoff between user offloading and cross-tier interference avoidance. By applying the tools of stochastic geometry, the uplink ASE is analytically derived as a function of the bias factor for the multichannel HCNs. The optimal bias factor can be obtained numerically by maximizing the system ASE. It is shown that the ASE performance analysis agrees with computer simulation very well. The results demonstrate that the proposed scheme can substantially improve the ASE performance of the multichannel HCNs for different small cell densities and outperform upon an existing biased cell association scheme.

INDEX TERMS Heterogeneous cellular network, multichannel, biased association, interference avoidance, stochastic geometry.

I. INTRODUCTION

Heterogeneous networks with massive small cells (SCs) overlaying macrocells have great potential for increasing data rate manyfold to meet the ever increasing demand of data traffic in wireless communications [1], [2]. However, the bandwidth sharing and densification of SCs cause serious co-tier and cross-tier interferences, which form barriers to boost spectral efficiency in heterogeneous cellular networks (HCNs) [3], [4]. It is well known that the interference signal strength is dependent on the system configuration, such as spatial node distributions, transmit power control, and channel propagation characteristics. Therefore, the development of an accurate performance analysis in terms of system parameters is important for the network management and design [5].

Stochastic geometry is a powerful tool for the performance analysis of large-scale wireless networks, where multiple active network devices are scattered irregularly with a high level of spatial randomness [6]. To facilitate the development of an analytical performance expression relating to signal-to-interference-plus-noise ratio (SINR) in HCNs, the stochastic geometry are usually deployed to characterize the spatial randomness of base stations (BSs) and users [7]. The benefit of the analytical expression is its great efficiency on the system performance evaluation upon the time-consuming system-level simulation. As a simple and effective stochastic model,

the Poisson point process (PPP) is widely used to model the random locations of base stations (BSs) and mobile terminals in HCNs, where massive small cell base stations (SBSs) and users are active in communication [8], [9].

It has been shown that the PPP model can provide a tight approximation of the system performance for both single-tier wireless networks [10] and multi-tier HCNs [11]. Under the assumption that the locations of macrocell base stations (MBSs) and SBSs are characterized by two independent spatial homogeneous PPPs, the successful transmission probability was developed for HCNs using orthogonal and shared subchannel deployments in [12]. Cheng *et al.* [13] derived the downlink throughput of cognitive SC networks with perfect sensing, where the locations of SBSs were modeled as a homogeneous PPP. By applying the stochastic geometry, the downlink coverage probability was evaluated for two-tier HCNs under the maximum SINR association and asynchronous transmissions in [14].

The works mentioned above focus on the downlink of HCNs, where all the BSs of the same tier have a unique transmit power. In the uplink, power control is generally leveraged to compensate for path loss [15]. Besides, when the users do not have enough power to support power control, they can only transmit with their maximum powers in wireless cellular networks (e.g., LTE-Advanced networks [16]). This location dependent power control policy introduces a new source of randomness related to the propagation distance between users and their serving BSs. In addition, unlike the downlink case, the location of the user of interest may be farther away than an interfering user from its serving BS in the uplink transmission. Therefore, the analysis of downlink cannot be directly applied to the uplink. Generally, in the case of using transmit power control and random mobile terminal locations, the uplink performance analysis in HCNs is more complicated than its downlink counterpart.

Chandrasekhar and Andrews [17] studied the uplink spectral efficiency of a two-tier HCN. For analytical tractability, it was considered that all interfering small cell users (SUs) were transmitting at the maximum power in the characterization of interference, which exaggerates the interference power level and thus underestimates the capacity in the realistic HCNs. In [18], the uplink outage probability and spectral efficiency were developed accounting for the truncated channel inversion power control strategy and the conventional cell association of using the strongest downlink received signal strength. However, under this power control scheme, the users, who are close to the macrocell edge, are in outage all the time. Furthermore, because of the large difference in transmit power between the MBS and SBS, the conventional maximum received signal power association scheme leads to heavily unbalanced traffic loads in the cellular tiers, limiting the full benefits of SCs. Thus, biased cell association was introduced in [19] and [20] to reshape the SC coverage adaptively in HCNs. By taking both biased association and power control into consideration, the authors in [21] derived an uplink rate distribution for HCNs. However, per user maximum transmit power constraint was neglected in [21] for simplifying the derivation, which is clearly far from the case of real-world transmissions. Besides, the analyses in [17], [18], and [21] are only applicable to fully loaded SCs and macrocells. However, the full load condition for each cell in realistic HCNs is too restrictive, especially for the SCs with small coverage and sufficient spectrum resource. According to the spatial patterns of different network components, the number of users associated with each cell depends on the bias factor and infrastructure density. Since the SINR and traffic loads are highly correlated, it is important to study the performance of multichannel HCNs with variable number of users per cell.

Compared to the aforementioned studies, the multichannel HCN considered in this paper differs in two key features. Firstly, the subchannels of the multichannel HCN are not fully utilized in light-load SCs. Due to the random locations of users, the number of associated users in each SC can vary greatly. Thus, the numbers of users served by some cells could be smaller than the available subchannels. Secondly, an adaptive subchannel allocation scheme is exploited to mitigate inter-cell interference in multichannel HCNs. It is known that cross-tier interference from macrocell users (MUs) affects the reception of SBSs severely in the uplink, especially for the MUs close to the SCs [22], [23] under channel inverse power control. In this paper, an effective SC interference mitigation scheme is proposed to avoid reusing the subchannels occupied by the nearby MUs that might transmit signals to their faraway MBSs with high powers.

The contributions of this paper can be summarized as follows:

1) An analytical framework of uplink area spectral efficiency (ASE) of multichannel HCNs with per user power control, maximum transmit power constraint, biased cell association, and cross-tier interference avoidance (CTIA) is developed. In this development, more practical components are considered in the performance analysis in comparing with existing works. Thus, the theoretical analysis derived in this paper will give more useful insight into the design of HCN. It is worth mentioning that none of the prior works has integrated all these components in the performance analysis of HCNs.
2) A coordinated subchannel selection scheme is proposed to reduce the cross-tier interference from MUs to SCs, of which each SC avoids choosing the subchannels occupied by nearby MUs according to its own traffic loads. Furthermore, the distribution of the guard radius of the no cross-tier interference zone for SCs is derived by using the theory of order statistics. To the best of our knowledge, this method is newly proposed for the uplink performance analysis of multichannel HCNs.
3) According to the statistics of system parameters, an analytical expression of ASE of multichannel HCN, which deploys biased cell association with the

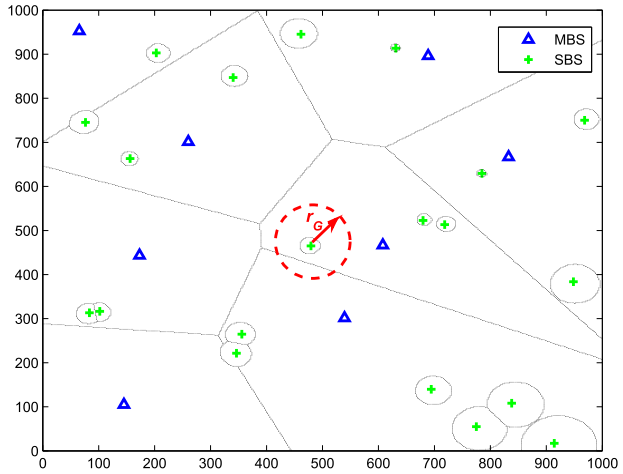

FIGURE 1. An illustration of a two-tier HCN coverage boundaries in an area of 1000m ×1000m, where the MBS and SBS locations are distributed as two independent PPPs.

proposed coordinated subchannel selection and channel inversion power control, is derived by applying the tools of stochastic geometry. Based on the derived results, the optimal network-specific bias factor can be obtained by maximizing the ASE via numerical methods. The optimal bias factor can make a good tradeoff between the traffic load balance and cross-tier interference mitigation, which is in contrast to the existing minimum path loss association in [21]. It is shown by simulation that the newly developed theoretical analysis is accurate and agreeable with computer simulations. Evaluation also shows that the proposed scheme is able to boost the system ASE considerably.

The rest of this paper is organized as follows. Section II describes the system model, including biased cell association, uplink power control, and SC subchannel selection policy. Equivalent user density, distribution of transmit power, statistics of guard radius, and success probability are derived in Section III. Section IV presents simulation results and discussions. In Section V, conclusions are given.

II. SYSTEM MODEL

As shown in Fig. 1, a two-tier HCN is considered in this paper, where the MBSs, SBSs, and users are spatially distributed according to independent 2-D homogeneous PPPs $\Psi_M = \{x_m^{(M)}, m = 1, 2, \ldots\}$, $\Psi_S = \{x_s^{(S)}, s = 1, 2, \ldots\}$, and Ψ_U, respectively. The densities, which are defined as the average numbers of points per unit area, of Ψ_M, Ψ_S, and Ψ_U are μ_M, μ_S, and μ_U, respectively. The macrocells and SCs share the same subchannel set of size N.

1) BIASED CELL ASSOCIATION

To solve the load imbalance between macrocell and SCs, biased cell association is adopted in the two-tier HCN. The connection principle is that a user is connected to the BS from which the biased received signal strength is the strongest. That is, an arbitrary user located at y is connected to the macrocell tier if

$$P_M \Delta_M \left(\min_{x_m^{(M)}} \|x_m^{(M)} - y\| \right)^{-\alpha_M} \geq P_S \Delta_S \left(\min_{x_s^{(S)}} \|x_s^{(S)} - y\| \right)^{-\alpha_S}, \quad (1)$$

where α_M and α_S are the path loss exponents from users to MBSs and SBSs, respectively, Δ_M and Δ_S are the bias factors of macrocells and SCs, respectively, P_M and P_S are downlink reference signal powers of macrocells and SCs, respectively, $x_m^{(M)}$ and $x_s^{(S)}$ are the locations of the m-th MBS and s-th SBS, respectively; otherwise, the user is associated with the nearest SBS.

Hereafter, "$\tau = M$" and "$\tau = S$" are referred to as the macrocell tier and the SC tier, respectively.

2) UPLINK POWER CONTROL

The channel model considered in this paper is a composite channel characterized by small scale fading and path loss. The channel gain from user u to its serving BS in the τ ($\in \{M, S\}$) tier is expressed as $d_u^{-\alpha_\tau} g_u$, where d_u is the propagation distance between user u and its serving BS, and g_u is the small scale fading coefficient assumed to be exponentially distributed with unit mean (i.e., Rayleigh fading). In the HCN, a target average received power level P_{th} at the serving BS is maintained in order to provide a desired quality of service for users at various locations. To achieve this goal, full channel inversion power control is deployed. Furthermore, the user transmission power is limited by the maximum power budget $P_{U,\max}$. Then, the transmit power of user u associated with the τ tier is expressed as

$$P_u^{(\tau)} = \min\{P_{th} d_u^{\alpha_\tau},\ P_{U,\max}\},\ \tau \in \{M, S\}. \quad (2)$$

3) COORDINATED SUBCHANNEL ALLOCATION

There are N available subchannels shared by macrocells and SCs transmissions in the HCN. In order to avoid intra-cell interference, a subchannel is assigned to no more than one user per cell. Due to the fact that an interfering MU may locate closely to the SBS of interest or have large transmit power when its location is far from its receiving MBS, the SCs may suffer from serious cross-tier interference from the macrocell tier. Let $\tilde{N}_{A,S} > 0$ denote the number of users in an active SC. When $\tilde{N}_{A,S} < N$, the SC can alleviate the cross-tier interference in a simple way by choosing the $\tilde{N}_{A,S}$ subchannels used by the most faraway interfering MUs or idle subchannles. It can be implemented by measuring the signal strength of individual subchannels at the SCs during the transmission of uplink pilot signals by MUs. Under this subchannel allocation policy, there will be a zone of no cross-tier interference around each SBS. The statistics of the radius r_G of the disc without cross-tier interference will be analyzed in Section III. In case the number of users in a cell is larger than N, N users are selected to transmit by using the round-robin policy and each active user is assigned one subchannel randomly.

4) SINR EXPRESSION

The instantaneous SINR of the received signal from typical user u at its serving BS (called tagged BS) in the τ tier can be expressed as

$$\mathrm{SINR}_{\tau,u} = \frac{P_u^{(\tau)} g_u d_u^{-\alpha_\tau}}{I_{M,\tau} + I_{S,\tau} + \sigma_v^2}, \tag{3}$$

where

$$I_{M,\tau} = \sum_{i \in \tilde{\Psi}_U^M \setminus \{u\}} P_i^{(M)} g_{M,i} r_{M,i}^{-\alpha_\tau}, \tag{4}$$

$$I_{S,\tau} = \sum_{j \in \tilde{\Psi}_U^S \setminus \{u\}} P_j^{(S)} g_{S,j} r_{S,j}^{-\alpha_\tau} \tag{5}$$

are the cumulative interference coming from interfering MUs and SUs, respectively, $\tilde{\Psi}_U^M$ and $\tilde{\Psi}_U^S$ are the point processes of all active MUs and SUs using the same subchannel as that of the typical user, respectively, $r_{\tau,i}$ is the distance between the interfering user i in the τ tier and the tagged BS, $g_{\tau,i}$ is the small scale fading coefficient, and σ_v^2 is the noise power.

It is noted that $\tilde{\Psi}_U^M$ and $\tilde{\Psi}_U^S$ are not strict PPPs because of the correlation between active users and BSs. For mathematical tractability, $\tilde{\Psi}_U^M$ and $\tilde{\Psi}_U^S$ are approximated as PPPs in the ASE analysis in the next section.

III. ASE PERFORMANCE ANALYSIS

In this section, an analytical expression of the ASE of the multichannel HCN is derived. Because the statistical property of the ASE for each subchannel is identical, we only focus on the performance analysis of the subchannel used by a typical user without loss of generality. The ASE of a typical subchannel can be expressed as

$$\mathrm{ASE} = \sum_{\tau \in \{M,S\}} \lambda_\tau \Pr\{\mathrm{SINR}_{\tau,u} \geq \varepsilon\} \log_2(1+\varepsilon), \tag{6}$$

where λ_τ is the equivalent user density of the τ tier, ε is a predefined SINR threshold, and $\Pr\{\mathrm{SINR}_{\tau,u} \geq \varepsilon\}$ is the success probability of user u in the τ tier.

For the development of the ASE expression, we need to derive the equivalent user density λ_τ and the success probability of user u, $\Pr\{\mathrm{SINR}_{\tau,u} \geq \varepsilon\}$. In the derivation of $\Pr\{\mathrm{SINR}_{\tau,u} \geq \varepsilon\}$, the statistics of transmit power $P_u^{(\tau)}$ and guard radius r_G are required to formulate the probabilities of success events.

A. THE EQUIVALENT ACTIVE USER DENSITY λ_τ

1) THE DERIVATION OF CELL ASSOCIATION PROBABILITY Λ_τ

Based on the association policy in Section II, the probability of a user associated with the τ tier is given by

$$\Lambda_\tau = \Pr\left\{P_\tau \Delta_\tau (X^{(\tau)})^{-\alpha_\tau} \geq P_{\bar{\tau}} \Delta_{\bar{\tau}} (X^{(\bar{\tau})})^{-\alpha_{\bar{\tau}}}\right\}, \quad \bar{\tau} \in \{M,S\} \setminus \{\tau\}, \tag{7}$$

where $X^{(\tau)} = \min_{x_b^{(\tau)} \in \Psi_\tau} \|x_b^{(\tau)} - y\|$, $\tau \in \{M,S\}$. The probability density function (pdf) of $X^{(\tau)}$ can be derived by differentiating the null probability of a PPP as [24]

$$f_{X^{(\tau)}}(x) = 2\pi\mu_\tau x \exp\{-\pi\mu_\tau x^2\}, \ \tau \in \{M,S\}. \tag{8}$$

Since $f_{X^{(M)}}(x)$ and $f_{X^{(S)}}(x)$ are independent, (7) can be further written as

$$\begin{aligned}\Lambda_\tau &= \Pr\left\{X^{(\bar{\tau})} \geq \left(\frac{P_{\bar{\tau}} \Delta_{\bar{\tau}} (X^{(\tau)})^{\alpha_\tau}}{P_\tau \Delta_\tau}\right)^{\frac{1}{\alpha_{\bar{\tau}}}}\right\} \\ &= \int_0^\infty \int_{\left(\frac{P_{\bar{\tau}} \Delta_{\bar{\tau}} x^{\alpha_\tau}}{P_\tau \Delta_\tau}\right)^{\frac{1}{\alpha_{\bar{\tau}}}}}^\infty f_{X^{(\bar{\tau})}}(y) f_{X^{(\tau)}}(x) \mathrm{d}y \mathrm{d}x \\ &= \int_0^\infty \exp\left\{-\pi\mu_{\bar{\tau}} \left(\frac{P_{\bar{\tau}} \Delta_{\bar{\tau}} x^{\alpha_\tau}}{P_\tau \Delta_\tau}\right)^{\frac{2}{\alpha_{\bar{\tau}}}}\right\} f_{X^{(\tau)}}(x) \mathrm{d}x. \end{aligned} \tag{9}$$

Special case $\alpha_M = \alpha_S$: When the two path loss exponents are equal, the cell association probability can be simplified as

$$\Lambda_\tau = \frac{\mu_\tau (P_\tau \Delta_\tau)^{\frac{2}{\alpha_\tau}}}{\mu_{\bar{\tau}} (P_{\bar{\tau}} \Delta_{\bar{\tau}})^{\frac{2}{\alpha_\tau}} + \mu_\tau (P_\tau \Delta_\tau)^{\frac{2}{\alpha_\tau}}}, \quad \tau \in \{M,S\}. \tag{10}$$

2) THE DENSITY OF ACTIVE USERS PER SUBCHANNEL

Based on the analysis above, the users can be divided into two disjoint subsets, i.e., the MU location set Ψ_U^M and the SU location set Ψ_U^S. Since an individual user in Ψ_U belongs to either Ψ_U^M or Ψ_U^S, the probabilities Λ_M and Λ_S can be viewed as the average fraction of users belonging to the point sets Ψ_U^M and Ψ_U^S, respectively [25]. It is known that the equivalent density of active users is affected by traffic load per cell, which in turn depends on the corresponding association area. Currently, the exact statistic of association area is still unknown. However, by using the association area approximation in [26]–[28], the probability mass function (pmf) of l users connected to one BS in the τ tier is given by

$$\Pr(N_\tau = l) = \frac{3.5^{3.5} \Gamma(3.5+l) (\Lambda_\tau \mu_U / \mu_\tau)^l}{l! \Gamma(3.5) (\Lambda_\tau \mu_U / \mu_\tau + 3.5)^{l+3.5}}, \tag{11}$$

where $\Gamma(a) = \int_0^\infty x^{a-1} e^{-x} \mathrm{d}x$ is the gamma fuction.

To avoid the intra-cell interference, there is at most one active user per subchannel in one Voronoi cell scheduled for a time slot, which results in some correlation across the locations of active users per subchannel and makes an exact description of active user locations unavailable. To facilitate the development of analytical performance expressions, the active user locations are usually approximated as PPP. It is worth mentioning that this approximation is widely used in the uplink performance analysis of HCNs, and the theoretical results derived under the approximation have been verified to match simulations very well in [26], [29], and [30].

With the pmf of user numbers per cell in (11), the probability that one subchannel is occupied by a user of a cell in the τ tier is given by

$$\begin{aligned} p_{A,\tau} &= \sum_{l=0}^{N} \Pr(N_\tau = l) \cdot \frac{l}{N} + \sum_{l=N+1}^{\infty} \Pr(N_\tau = l) \\ &= 1 - \sum_{l=0}^{N} \Pr(N_\tau = l) \cdot \frac{N-l}{N}. \end{aligned} \tag{12}$$

Accordingly, the point process of all the active users in the τ tier sharing the same subchannel with the typical user, $\tilde{\Psi}_U^{\tau}$, can be approximated as a thinned PPP in the τ tier, and the density of active users per subchannel is the product of the cell density and the probability that one channel being occupied by a user of a cell, expressed as

$$\lambda_\tau = \mu_\tau p_{A,\tau},\ \tau \in \{M, S\}. \tag{13}$$

B. THE DISTRIBUTION OF TRANSMIT POWER $P_u^{(\tau)}$

Due to uplink power control, the transmit power depends on the distance from the user to its serving BS. In order to obtain the distribution of the transmit power, we need to derive the pdf of the propagation distance of the connection link.

1) THE PDF OF THE PROPAGATION DISTANCE OF THE CONNECTION LINK

Assuming the serving BS is in the τ tier, the cumulative distribution function (cdf) of the propagation distance D_τ can be expressed as

$$\begin{aligned} F_{D_\tau}(d) &= \Pr\{D_\tau \le d\} \\ &= \Pr\left\{X^{(\tau)} \le d \mid P_\tau \Delta_\tau \left(X^{(\tau)}\right)^{-\alpha_\tau} \ge P_{\bar{\tau}} \Delta_{\bar{\tau}} \left(X^{(\bar{\tau})}\right)^{-\alpha_{\bar{\tau}}}\right\} \\ &= \frac{\Pr\left\{X^{(\tau)} \le d, P_\tau \Delta_\tau \left(X^{(\tau)}\right)^{-\alpha_\tau} \ge P_{\bar{\tau}} \Delta_{\bar{\tau}} \left(X^{(\bar{\tau})}\right)^{-\alpha_{\bar{\tau}}}\right\}}{\Pr\{P_\tau \Delta_\tau \left(X^{(\tau)}\right)^{-\alpha_\tau} \ge P_{\bar{\tau}} \Delta_{\bar{\tau}} \left(X^{(\bar{\tau})}\right)^{-\alpha_{\bar{\tau}}}\}} \\ &= \frac{\int_0^d \exp\left\{-\pi \mu_{\bar{\tau}} \left(\frac{P_{\bar{\tau}} \Delta_{\bar{\tau}} x^{\alpha_\tau}}{P_\tau \Delta_\tau}\right)^{\frac{2}{\alpha_{\bar{\tau}}}}\right\} f_{X^{(\tau)}}(x) \mathrm{d}x}{\Lambda_\tau}. \end{aligned} \tag{14}$$

Differentiating $F_{D_\tau}(d)$ with respect to (w.r.t.) d, the pdf of D_τ can be expressed as

$$f_{D_\tau}(d) = \frac{2\pi \mu_\tau d \exp\left\{-\pi \mu_\tau d^2 - \pi \mu_{\bar{\tau}} \left(\frac{P_{\bar{\tau}} \Delta_{\bar{\tau}} d^{\alpha_\tau}}{P_\tau \Delta_\tau}\right)^{\frac{2}{\alpha_{\bar{\tau}}}}\right\}}{\Lambda_\tau}. \tag{15}$$

Special Case $\alpha_M = \alpha_S$: When the two path loss exponents are equal, the cdf and pdf of D_τ can be further simplified as

$$F_{D_\tau}(d) = 1 - \exp\left\{-\pi \mu_{\bar{\tau}} \left(\frac{P_{\bar{\tau}} \Delta_{\bar{\tau}}}{P_\tau \Delta_\tau}\right)^{\frac{2}{\alpha_\tau}} d^2 - \pi \mu_\tau d^2\right\}, \tag{16}$$

$$f_{D_\tau}(d) = \frac{2\pi \mu_\tau d \exp\left\{-\pi \mu_{\bar{\tau}} \left(\frac{P_{\bar{\tau}} \Delta_{\bar{\tau}}}{P_\tau \Delta_\tau}\right)^{\frac{2}{\alpha_\tau}} d^2 - \pi \mu_\tau d^2\right\}}{\Lambda_\tau}. \tag{17}$$

2) THE CDF AND PDF OF TRANSMIT POWER $P_u^{(\tau)}$

Recalling the power control strategy in (2), the transmit power can be written as

$$P_u^{(\tau)} = \begin{cases} P_{th} D_\tau^{\alpha_\tau}, & 0 \le D_\tau < \left(P_{U,\max}/P_{th}\right)^{\frac{1}{\alpha_\tau}} \\ P_{U,\max}, & D_\tau \ge \left(P_{U,\max}/P_{th}\right)^{\frac{1}{\alpha_\tau}}. \end{cases} \tag{18}$$

It is shown in (18) that the transmit power is a mixed random variable (r.v.) consisting of continuous and discrete parts. The cdf of the transmit power of user u is given as

$$F_{P_u^{(\tau)}}(t) = \begin{cases} F_{D_\tau}\left(\left(\frac{t}{P_{th}}\right)^{\frac{1}{\alpha_\tau}}\right), & 0 \le t < P_{U,\max} \\ 1, & t \ge P_{U,\max}. \end{cases} \tag{19}$$

The corresponding pdf of $P_u^{(\tau)}$ can be expressed as

$$\begin{aligned} f_{P_u^{(\tau)}}(t) = &\frac{1}{\alpha_\tau P_{th}} \left(\frac{t}{P_{th}}\right)^{\frac{1-\alpha_\tau}{\alpha_\tau}} f_{D_\tau}\left(\left(\frac{t}{P_{th}}\right)^{\frac{1}{\alpha_\tau}}\right) \\ &+ \left[1 - F_{D_\tau}\left(\left(\frac{P_{U,\max}}{P_{th}}\right)^{\frac{1}{\alpha_\tau}}\right)\right] \delta(t - P_{U,\max}), \end{aligned} \tag{20}$$

for $0 \le t \le P_{U,\max}$, and zero, otherwise, where $\delta(t)$ is the Dirac delta function.

C. THE STATISTICS OF THE RADIUS OF CROSS-TIER INTERFERENCE AVOIDANCE ZONE

Defining $N_{A,S}$ as the number of active users connected to an SC, we have

$$\Pr\{N_{A,S} = l\} = \begin{cases} \Pr\{N_S = l\}, & 0 \le l < N \\ 1 - \sum_{i=0}^{N-1} \Pr\{N_S = i\}, & l = N. \end{cases} \tag{21}$$

where $\Pr\{N_S = l\}$ is given by (11).

It is known that when $N_{A,S} = 0$, there is no SU transmission in the SC. Thus, under the condition that there is at least one active SU, the pmf of the number of active users per SC is given by

$$\Pr\left\{\tilde{N}_{A,S} = n\right\} = \frac{\Pr\{N_{A,S} = n\}}{\sum_{l=1}^{N} \Pr\{N_{A,S} = l\}}, \quad 1 \le n \le N. \tag{22}$$

When an SC selects $\tilde{N}_{A,S}$ out of N subchannels for transmissions, it avoids selecting the subchannels used by the $(N - \tilde{N}_{A,S})$ nearest MUs in order to mitigate the severe cross-tier interference. Then, the guard radius of the disc without cross-tier interference for the tagged SBS is given by

$$r_G = \min\{r_{\min,1}, \ldots, r_{\min,N}\}_{N - \tilde{N}_{A,S}+1}, \tag{23}$$

where $r_{\min,n}$ denotes the minimum distance between the tagged SBS and the active MUs on the nth subchannel, and $\min\{\cdot\}_k$ denotes the kth smallest value in the set $\{\cdot\}$.

Recalling that the locations of the active MUs per subchannel is modeled as a thinned PPP with the density of λ_M in (13), the pdf of $r_{\min,n}$ is given by [24]

$$f_{r_{\min,n}}(\rho) = 2\pi \lambda_M \rho \exp\left\{-\pi \lambda_M \rho^2\right\}. \tag{24}$$

The cdf of $r_{\min,n}$ is given as

$$F_{r_{\min,n}}(\rho) = \Pr\{r_{\min,n} < \rho\} = \exp\left\{-\pi \lambda_M \rho^2\right\}. \tag{25}$$

Since $\{r_{\min,n}\}$ are independent and identically distributed random variables, the conditional cdf of r_G can be obtained by using the theory of order statistics as

$$\begin{aligned} F_{r_G}(\rho|\tilde{N}_{A,S}=n) &= \Pr\{r_G<\rho|\tilde{N}_{A,S}=n\} \\ &= \sum_{l=N-n+1}^{N}\binom{N}{l}\left(1-\exp\left\{-\pi\lambda_M\rho^2\right\}\right)^l \\ &\quad\times\left(\exp\left\{-\pi\lambda_M\rho^2\right\}\right)^{N-l}. \end{aligned} \tag{26}$$

Differentiating the conditional cdf w.r.t. ρ gives the conditional pdf of r_G as

$$\begin{aligned} f_{r_G}(\rho|\tilde{N}_{A,S}=n) &= \tfrac{2\pi\lambda_M\rho(N!)}{(n-1)!(N-n)!}\left(1-\exp\left\{-\pi\lambda_M\rho^2\right\}\right)^{N-n} \\ &\quad\times\left(\exp\left\{-\pi\lambda_M\rho^2\right\}\right)^{n}. \end{aligned} \tag{27}$$

Thus, the marginal pdf of r_G is expressed as

$$f_{r_G}(\rho)=\sum_{n=1}^{N} f_{r_G}(\rho|\tilde{N}_{A,S}=n)\Pr\{\tilde{N}_{A,S}=n\}. \tag{28}$$

The statistics of transmit power and the radius of no cross-tier interference zone, which have been respectively developed in Subsections III-B and III-C, can facilitate the derivation of success probability in the next subsection.

D. THE DERIVATION OF SUCCESS PROBABILITY $\Pr\{SINR_{\tau,u}\geq\varepsilon\}$

In this subsection, the analysis of success probability is conducted on the typical user. Based on Slivnyak's theorem, the analysis also holds for any active users [32], [33]. According to the power control scheme given in (2), it is shown in Subsection III-B.2 that the transmit power is a mixed r.v.. Using the total probability conditioned on the transmit power, the success probability $\Pr\{\mathrm{SINR}_{\tau,u}\geq\varepsilon\}$ can be expressed as

$$\Pr\{\mathrm{SINR}_{\tau,u}\geq\varepsilon\}=O_{\tau,1}+O_{\tau,2} \tag{29}$$

with

$$\begin{aligned} O_{\tau,1} &= \Pr\{\mathrm{SINR}_{\tau,u}\geq\varepsilon|0\leq P_u^{(\tau)}<P_{U,\max}\} \\ &\quad\times\Pr\{0\leq P_u^{(\tau)}<P_{U,\max}\}, \end{aligned} \tag{30}$$

$$O_{\tau,2} = \Pr\{\mathrm{SINR}_{\tau,u}\geq\varepsilon|P_u^{(\tau)}=P_{U,\max}\}\Pr\{P_u^{(\tau)}=P_{U,\max}\}. \tag{31}$$

1) THE CALCULATIONS OF $O_{\tau,1}$ AND $O_{\tau,2}$

In the case of $0\leq P_\tau^{(u)}<P_{U,\max}$, $O_{\tau,1}$ can be expressed as

$$\begin{aligned} O_{\tau,1} &= F_{D_\tau}\left(\left(\tfrac{P_{U,\max}}{P_{th}}\right)^{\frac{1}{\alpha_\tau}}\right)\Pr\{P_{th}g_u\geq\varepsilon(\sigma_v^2+I_{M,\tau}+I_{S,\tau})\} \\ &= F_{D_\tau}\left(\left(\tfrac{P_{U,\max}}{P_{th}}\right)^{\frac{1}{\alpha_\tau}}\right)\mathbb{E}\left\{\exp\left\{\tfrac{-\varepsilon(\sigma_v^2+I_{M,\tau}+I_{S,\tau})}{P_{th}}\right\}\right\} \\ &= F_{D_\tau}\left(\left(\tfrac{P_{U,\max}}{P_{th}}\right)^{\frac{1}{\alpha_\tau}}\right)\exp\left\{\tfrac{-\varepsilon\sigma_v^2}{P_{th}}\right\} \\ &\quad\times\mathcal{L}_{I_{M,\tau}}\left(\tfrac{\varepsilon}{P_{th}}\right)\mathcal{L}_{I_{S,\tau}}\left(\tfrac{\varepsilon}{P_{th}}\right) \end{aligned} \tag{32}$$

where $\mathcal{L}_{\tau,\tau'}(\phi)$, $\tau\in\{M,S\}$ is the Laplace transform (LT) of the cumulative interference from the interfering users of τ tier onto the tagged BS in the τ' tier evaluated at ϕ.

In the case of $P_u^{(\tau)}=P_{U,\max}$, the user transmits with the maximum power, and thus the received power at the tagged BS depends on the propagation distance from the typical user to the tagged BS. Based on the pdf of the connection distance D_u in (15) and (17), $O_{\tau,2}$ can be expressed as

$$\begin{aligned} &O_{\tau,2} \\ &= \int_{\left(\frac{P_{U,\max}}{P_{th}}\right)^{\frac{1}{\alpha_\tau}}}^{\infty}\Pr\left\{P_{U,\max}g_u d_u^{-\alpha_\tau}\geq\varepsilon\left(\sigma_v^2+I_{M,\tau}+I_{S,\tau}\right)\right\} \\ &\quad\times f_{D_\tau}(d_u)\mathrm{d}d_u \\ &= \int_{\left(\frac{P_{U,\max}}{P_{th}}\right)^{\frac{1}{\alpha_\tau}}}^{\infty}\mathbb{E}\left\{\exp\left\{\tfrac{-\varepsilon(\sigma_v^2+I_{M,\tau}+I_{S,\tau})}{P_{U,\max}d_u^{-\alpha_\tau}}\right\}\right\}f_{D_\tau}(d_u)\mathrm{d}d_u \\ &= \int_{\left(\frac{P_{U,\max}}{P_{th}}\right)^{\frac{1}{\alpha_\tau}}}^{\infty}\exp\left\{\tfrac{-\varepsilon\sigma_v^2}{P_{U,\max}d_u^{-\alpha_\tau}}\right\}\mathcal{L}_{I_{M,\tau}}\left(\tfrac{\varepsilon}{P_{U,\max}d_u^{-\alpha_\tau}}\right) \\ &\quad\times\mathcal{L}_{I_{S,\tau}}\left(\tfrac{\varepsilon}{P_{U,\max}d_u^{-\alpha_\tau}}\right)f_{D_\tau}(d_u)\mathrm{d}d_u. \end{aligned} \tag{33}$$

Since $\tilde{\Psi}_U^\tau\setminus\{u\}$ is a reduced Palm point process w.r.t. the original PPP $\tilde{\Psi}_U^\tau$, it is still a PPP with the same density as the original PPP for a sufficiently large number of points. The calculation of $\left\{\mathcal{L}_{I_{\tau,\tau'}}(\phi);\ \tau,\tau'\in\{M,S\}\right\}$ can be expressed as

$$\begin{aligned} \mathcal{L}_{I_{\tau,\tau'}}(\phi) &= \mathbb{E}\left\{\exp\{-\phi I_{\tau,\tau'}\}\right\} \\ &= \mathbb{E}\left\{\exp\{-\phi\sum_{i\in\tilde{\Psi}_U^\tau}P_i^{(\tau)}g_{\tau,i}r_{\tau,i}^{-\alpha_{\tau'}}\}\right\} \\ &= \mathbb{E}\left\{\prod_{i\in\tilde{\Psi}_U^\tau}\mathbb{E}_{g_{\tau,i}}\left\{\exp\{-\phi P_i^{(\tau)}g_{\tau,i}r_{\tau,i}^{-\alpha_{\tau'}}\}\right\}\right\} \\ &= \mathbb{E}\left\{\prod_{i\in\tilde{\Psi}_U^\tau}\frac{1}{1+\phi P_i^{(\tau)}r_{\tau,i}^{-\alpha_{\tau'}}}\right\}, \end{aligned} \tag{34}$$

where the last expression is obtained by making use of the unit mean exponential pdfs of $\{g_{\tau,i}\}$ and their independence of the locations of the interfering users in $\tilde{\Psi}_U^\tau$.

By applying the probability generating functional (PGFL) of PPPs in [32] and [33], (34) can be expressed further in the next subsections. Because of the effects of coordinated subchannel allocation policy, the evaluation method of $\mathcal{L}_{I_{M,S}}$ is different from others, namely, $\mathcal{L}_{I_{M,M}}$, $\mathcal{L}_{I_{S,S}}$, $\mathcal{L}_{I_{S,M}}$. Therefore, $\{\mathcal{L}_{I_{\tau,\tau'}}\}$ are evaluated via two different approaches in the following.

2) THE CALCULATION OF $\mathcal{L}_{I_{M,M}}$, $\mathcal{L}_{I_{S,S}}$, $\mathcal{L}_{I_{S,M}}$

Let $I_{\tau,\tau'}$ be cumulative interference denoting $\{I_{M,M}, I_{S,S}, I_{S,M}\}$. Due to the association rule in (1), the distance from the interfering user i to the tagged BS should satisfy

$$r_{\tau,i}\geq\left(\tfrac{P_{\tau'}\Delta_{\tau'}d_i^{\alpha_\tau}}{P_\tau\Delta_\tau}\right)^{\frac{1}{\alpha_{\tau'}}}\geq\left(\tfrac{P_{\tau'}\Delta_{\tau'}P_i^{(\tau)}}{P_\tau\Delta_\tau P_{th}}\right)^{\frac{1}{\alpha_{\tau'}}}, \tag{35}$$

$$\begin{aligned}\mathcal{L}_{I_{\tau,\tau'}}(\phi) &= \exp\left\{-2\pi\lambda_\tau \int_0^\infty \int_{(\frac{P_{\tau'}\Delta_{\tau'}P_i^{(\tau)}}{P_\tau\Delta_\tau P_{th}})^{\frac{1}{\alpha_\tau}}}^\infty \frac{\phi P_i^{(\tau)} r_{\tau,i}^{-\alpha_{\tau'}}}{1+\phi P_i^{(\tau)} r_{\tau,i}^{-\alpha_{\tau'}}} r_{\tau,i} \mathrm{d}r_{\tau,i} f_{D_\tau}(d_i)\mathrm{d}d_i\right\} \\ &= \exp\left\{-2\pi\lambda_\tau \int_0^{(\frac{P_{U,\max}}{P_{th}})^{\frac{1}{\alpha_\tau}}} \int_{(\frac{P_{\tau'}\Delta_{\tau'}P_i^{(\tau)}}{P_\tau\Delta_\tau P_{th}})^{\frac{1}{\alpha_\tau}}}^\infty \frac{\phi P_i^{(\tau)} r_{\tau,i}^{-\alpha_{\tau'}}}{1+\phi P_i^{(\tau)} r_{\tau,i}^{-\alpha_{\tau'}}} r_{\tau,i} \mathrm{d}r_{\tau,i} f_{D_\tau}(d_i)\mathrm{d}d_i \right. \\ &\quad \left. -2\pi\lambda_\tau \int_{(\frac{P_{U,\max}}{P_{th}})^{\frac{1}{\alpha_\tau}}}^\infty \int_{(\frac{P_{\tau'}\Delta_{\tau'}P_{U,\max}}{P_\tau\Delta_\tau P_{th}})^{\frac{1}{\alpha_\tau}}}^\infty \frac{\phi P_{U,\max} r_{\tau,i}^{-\alpha_{\tau'}}}{1+\phi P_{U,\max} r_{\tau,i}^{-\alpha_{\tau'}}} r_{\tau,i} \mathrm{d}r_{\tau,i} f_{D_\tau}(d_i)\mathrm{d}d_i\right\} \end{aligned} \tag{36}$$

where the last inequality exploits the fact of the power control in (2) that $P_i^{(\tau)} \le P_{th} d_i^{\alpha_\tau}$. Then, by using the PGFL of PPPs, the LT $\mathcal{L}_{I_{\tau,\tau'}}$ can be further written as (36), shown at the top of this page.

The first term in the exponent of (36) is for the case of $P_i^{(\tau)} < P_{U,\max}$, while the second term is for $P_i^{(\tau)} = P_{U,\max}$. For the first term with $P_i^{(\tau)} < P_{U,\max}$, we have $P_i^{(\tau)} = P_{th} d_i^{\alpha_\tau}$. Substituting this transmit power into the first term of (36), $\mathcal{L}_{I_{\tau,\tau'}}(\phi)$ is expressed as

$$\begin{aligned}&\mathcal{L}_{I_{\tau,\tau'}}(\phi) \\ &= \exp\left\{-2\pi\lambda_\tau \int_0^{P_{U,\max}} \int_{(\frac{P_{\tau'}\Delta_{\tau'}P_i^{(\tau)}}{P_\tau\Delta_\tau P_{th}})^{\frac{1}{\alpha_\tau}}}^\infty \right. \\ &\quad \times \frac{\phi P_i^{(\tau)} r_{\tau,i}^{-\alpha_{\tau'}}}{1+\phi P_i^{(\tau)} r_{\tau,i}^{-\alpha_{\tau'}}} r_{\tau,i} \mathrm{d}r_{\tau,i} f_{P_i^{(\tau)}}\left(P_i^{(\tau)}\right) \mathrm{d}P_i^{(\tau)} \\ &\quad -2\pi\lambda_\tau \Pr\{P_i^{(\tau)} = P_{U,\max}\} \\ &\quad \left. \times \int_{(\frac{P_{\tau'}\Delta_{\tau'}P_{U,\max}}{P_\tau\Delta_\tau P_{th}})^{\frac{1}{\alpha_\tau}}}^\infty \frac{\phi P_{U,\max} r_{\tau,i}^{-\alpha_{\tau'}}}{1+\phi P_{U,\max} r_{\tau,i}^{-\alpha_{\tau'}}} r_{\tau,i} \mathrm{d}r_{\tau,i}\right\}. \end{aligned} \tag{37}$$

In order to further simplify the expression of (37), by substituting $\eta = r_{\tau,i}\left(\phi P_i^{(\tau)}\right)^{-\frac{1}{\alpha_{\tau'}}}$ into (37), we can get

$$\begin{aligned}\mathcal{L}_{I_{\tau,\tau'}}(\phi) = \exp\Bigg\{ &-2\pi\lambda_\tau \phi^{\frac{2}{\alpha_{\tau'}}} \int_0^{P_{U,\max}} \left(P_i^{(\tau)}\right)^{\frac{2}{\alpha_{\tau'}}} \\ &\times \mathcal{C}_{\tau,\tau'}\left(P_i^{(\tau)}\right) f_{P_i^{(\tau)}}\left(P_i^{(\tau)}\right) \mathrm{d}P_i^{(\tau)} \\ &-2\pi\lambda_\tau \phi^{\frac{2}{\alpha_{\tau'}}} \left(P_{U,\max}\right)^{\frac{2}{\alpha_{\tau'}}} \mathcal{C}_{\tau,\tau'}\left(P_{U,\max}\right) \\ &\times \Pr\left\{P_i^{(\tau)} = P_{U,\max}\right\}\Bigg\} \end{aligned} \tag{38}$$

with

$$\begin{aligned}&\mathcal{C}_{\tau,\tau'}(P_i^{(\tau)}) \\ &= \int_{\left(\frac{P_{\tau'}\Delta_{\tau'}P_i^{(\tau)}}{P_\tau\Delta_\tau P_{th}}\right)^{\frac{1}{\alpha_\tau}}}^\infty \left(\frac{1}{\phi P_i^{(\tau)}}\right)^{\frac{1}{\alpha_{\tau'}}} \frac{\eta}{1+\eta^{\alpha_{\tau'}}} \mathrm{d}\eta \\ &= \frac{1}{\alpha'_\tau - 2}\left[\frac{1}{\phi P_i^{(\tau)}}\left(\frac{P_{\tau'}\Delta_{\tau'}P_i^{(\tau)}}{P_\tau\Delta_\tau P_{th}}\right)^{\frac{\alpha_{\tau'}}{\alpha_\tau}}\right]^{\frac{2-\alpha_{\tau'}}{\alpha_{\tau'}}} \\ &\quad \times {}_2F_1\left(1, \frac{\alpha_{\tau'}-2}{\alpha_{\tau'}}; \frac{2\alpha_{\tau'}-2}{\alpha_{\tau'}}; -\phi P_i^{(\tau)}\left(\frac{P_\tau\Delta_\tau P_{th}}{P_{\tau'}\Delta_{\tau'}P_i^{(\tau)}}\right)^{\frac{\alpha_{\tau'}}{\alpha_\tau}}\right), \\ &\qquad \text{for } \alpha_{\tau'} > 2, \end{aligned} \tag{39}$$

where the last expression in (39) is obtained by using [34, eq. (3.194)], and ${}_2F_1(\cdot,\cdot;\cdot;\cdot)$ is the Gauss hypergeometric function.

Special case $\alpha_M = \alpha_S$: For $\alpha_\tau > 2$, $\mathcal{C}_{\tau,\tau'}(P_i^{(\tau)})$ becomes independent of $P_i^{(\tau)}$ as

$$\begin{aligned}&C_{\tau,\tau'} \triangleq \mathcal{C}_{\tau,\tau'}\left(P_i^{(\tau)}\right) \\ &= \int_{\left(\frac{P_{\tau'}\Delta_{\tau'}}{\phi P_\tau\Delta_\tau P_{th}}\right)^{\frac{1}{\alpha_\tau}}}^\infty \frac{\eta}{1+\eta^{\alpha_\tau}} \mathrm{d}\eta \\ &= \frac{1}{\alpha_\tau - 2}\left(\frac{P_{\tau'}\Delta_{\tau'}}{\phi P_\tau\Delta_\tau P_{th}}\right)^{\frac{2-\alpha_\tau}{\alpha_\tau}} {}_2F_1\left(1, \frac{\alpha_\tau-2}{\alpha_\tau}; \frac{2\alpha_\tau-2}{\alpha_\tau}; -\frac{\phi P_\tau\Delta_\tau P_{th}}{P_{\tau'}\Delta_{\tau'}}\right). \end{aligned} \tag{40}$$

Accordingly, the LT $\mathcal{L}_{I_{\tau,\tau'}}(\phi)$ in (38) can be expressed in a compact form as

$$\mathcal{L}_{I_{\tau,\tau'}}(\phi) = \exp\left\{-2\pi\lambda_\tau \phi^{\frac{2}{\alpha_{\tau'}}} C_{\tau,\tau'}\beta\right\} \tag{41}$$

with

$$\begin{aligned}\beta &= \int_0^{P_{U,\max}} \left(P_i^{(\tau)}\right)^{\frac{2}{\alpha_{\tau'}}} f_{P_i^{(\tau)}}\left(P_i^{(\tau)}\right) \mathrm{d}P_i^{(\tau)} \\ &\quad + P_{U,\max}^{\frac{2}{\alpha_{\tau'}}} \Pr\left\{P_i^{(\tau)} = P_{U,\max}\right\} \\ &= \frac{\pi\mu_\tau}{\Lambda_\tau\left[\pi\mu_{\bar\tau}\left(\frac{P_{\bar\tau}\Delta_{\bar\tau}}{P_\tau\Delta_\tau}\right)^{\frac{2}{\alpha_{\bar\tau}}} + \pi\mu_\tau\right]^2 \left(\frac{1}{P_{th}}\right)^{\frac{2}{\alpha_\tau}}} \\ &\quad \times \gamma\left(2, \left[\pi\mu_{\bar\tau}\left(\frac{P_{\bar\tau}\Delta_{\bar\tau}}{P_\tau\Delta_\tau}\right)^{\frac{2}{\alpha_{\bar\tau}}} + \pi\mu_\tau\right]\left(\frac{1}{P_{th}}\right)^{\frac{2}{\alpha_\tau}} P_{U,\max}^{\frac{2}{\alpha_\tau}}\right) \\ &\quad + P_{U,\max}^{\frac{2}{\alpha_{\tau'}}} \Pr\left\{P_i^{(\tau)} = P_{U,\max}\right\}, \end{aligned} \tag{42}$$

where $\gamma(a,b) = \int_0^b x^{a-1}e^{-x}\mathrm{d}x$ is the lower incomplete gamma function.

3) THE CALCULATION OF $\mathcal{L}_{I_{M,S}}$

Due to the interference coordination subchannel allocation scheme, the cross-tier interference at the tagged SBS stemming from MUs is reduced. Using the PGFL of PPPs and

the pdf of guard radius without cross-tier interference in (28), we have

$$\mathcal{L}_{I_{M,S}}(\phi) = \exp\{-2\pi\lambda_M \int_0^\infty \int_\rho^\infty \mathbb{E}_{P_i^{(M)}}\left\{\frac{\phi P_i^{(M)} r_{M,i}^{-\alpha_S}}{1+\phi P_i^{(M)} r_{M,i}^{-\alpha_S}}\right\} \times r_{M,i} f_{r_G}(\rho)\mathrm{d}r_{M,i}\mathrm{d}\rho\}. \quad (43)$$

Substituting $\eta = r_{M,i}\left(\phi P_i^{(M)}\right)^{-\frac{1}{\alpha_S}}$ into (43), we can get $\mathcal{L}_{I_{M,S}}$ in (44), shown at the bottom of this page, where the last expression in (44) is obtained by substituting (20) into the term $\mathbb{E}_{P_i^{(M)}}\{\cdot\}$, and $\mathcal{Q}\left(\rho, P_i^{(M)}\right)$ is expressed as

$$\begin{aligned}\mathcal{Q}\left(\rho, P_i^{(M)}\right) &= \int_{\rho\left(\phi P_i^{(M)}\right)^{-\frac{1}{\alpha_S}}}^\infty \frac{\eta}{1+\eta^{\alpha_S}}\mathrm{d}\eta \\ &= \frac{1}{\alpha_S-2}\left(\frac{\rho^{\alpha_S}}{\phi P_i^{(M)}}\right)^{\frac{2-\alpha_S}{\alpha_S}} {}_2F_1\left(1, \frac{\alpha_S-2}{\alpha_S}; \frac{2\alpha_S-2}{\alpha_S}; -\frac{\phi P_i^{(M)}}{\rho^{\alpha_S}}\right).\end{aligned} \quad (45)$$

In summary, the calculation of the LTs, $\{\mathcal{L}_{I_{\tau,\tau'}}\}$, can be carried out by using (38) (or (41)) and (44). Then, $O_{\tau,1}$ and $O_{\tau,2}$ of the success probability can be evaluated with $\{\mathcal{L}_{I_{\tau,\tau'}}\}$ via (32) and (33), respectively.

IV. SIMULATION AND NUMERICAL RESULTS

In this section, we present the ASE performance of the proposed scheme through numerical evaluation and computer simulation, where the optimal bias factor of SCs is obtained by a one-dimensional search method. Without loss of generality, the bias factor of macrocell is set as $\Delta_M = 1$. In simulations, we only focus on the adjustment of the SC bias factor. Other parameters used in the simulations are listed in Table 1.

TABLE 1. Simulation parameters.

Parameters	Values
Macrocell reference signal power P_M	46dBm
SC reference signal power P_S	23dBm
User maximum transmit power $P_{U,\max}$	20dBm
Noise power σ_v^2	-110dBm
Target received power P_{th}	-60dBm
SINR threshold ε	$0 \sim 10$dB
Macrocell path loss exponent α_M	3.5
SC path loss exponent α_S	3.5
Number of subchannels N	8
Density of MBSs μ_M	2×10^{-6}BSs/m^2
Density of SBSs μ_S	$10 \sim 80\mu_M$
Density of users μ_U	4×10^{-4}users/m^2

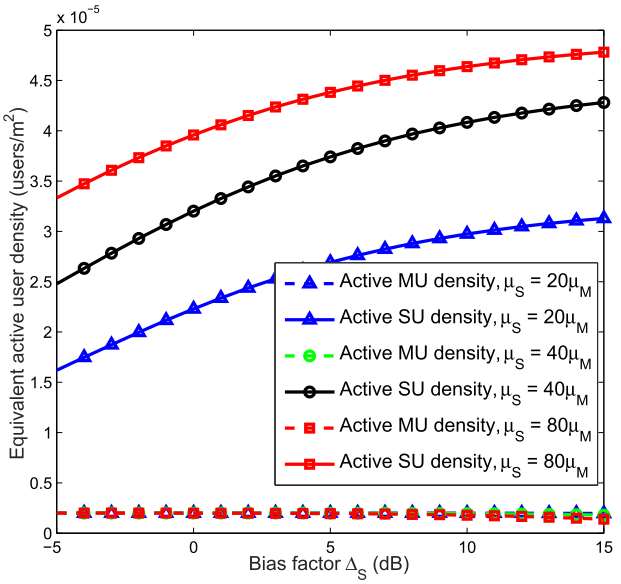

FIGURE 2. Per tier active user density versus bias factor Δ_S for different SC densities with $\varepsilon = 4$dB.

A. PER TIER ACTIVE USER DENSITY AND SUCCESS PROBABILITY

Figure 2 plots the equivalent active user density per subchannel in (13) for different SC densities. In the figure, the active SU density increases with the bias factor. It is because the association coverage per SC is expanded as the bias factor increases. The equivalent active MU density is almost unchanged as the bias factor increases, which is equal to the density of MBSs. The reason is that the macrocell coverage is much larger than that of SC and the number of users associated to each MBS is sufficiently large occupying nearly all the subchannels and giving $p_{A,M}$ in (13) close to one.

Figure 3 plots per tier success probability of users derived in (29). It is shown that the SU success probability is decreased as the bias factor increases. The reasons are twofold. Firstly, the number of associated users per SC is increased as the bias factor increases, and thus the number of subchannels that can be selected to avoid cross-tier interference is decreased. Secondly, the co-tier interference from interfering SCs becomes larger as per SC coverage

$$\begin{aligned}\mathcal{L}_{I_{M,S}}(\phi) &= \exp\left\{-2\pi\lambda_M\phi^{\frac{2}{\alpha_S}}\mathbb{E}_{P_i^{(M)}}\{(P_i^{(M)})^{\frac{2}{\alpha_S}}\int_0^\infty \mathcal{Q}(\rho, P_i^{(M)}) f_{r_G}(\rho)\mathrm{d}\rho\}\right\} \\ &= \exp\left\{-2\pi\lambda_M\phi^{\frac{2}{\alpha_S}}\int_0^{P_{U,\max}}\int_0^\infty (P_i^{(M)})^{\frac{2}{\alpha_S}}\mathcal{Q}(\rho, P_i^{(M)}) f_{r_G}(\rho) f_{P_i^{(M)}}(P_i^{(M)})\mathrm{d}\rho\mathrm{d}P_i^{(M)}\right. \\ &\quad \left.-2\pi\lambda_M\phi^{\frac{2}{\alpha_S}}P_{U,\max}^{\frac{2}{\alpha_S}}\Pr\{P_i^{(M)} = P_{U,\max}\}\int_0^\infty \mathcal{Q}(\rho, P_{U,\max}) f_{r_G}(\rho)\mathrm{d}\rho\right\}\end{aligned} \quad (44)$$

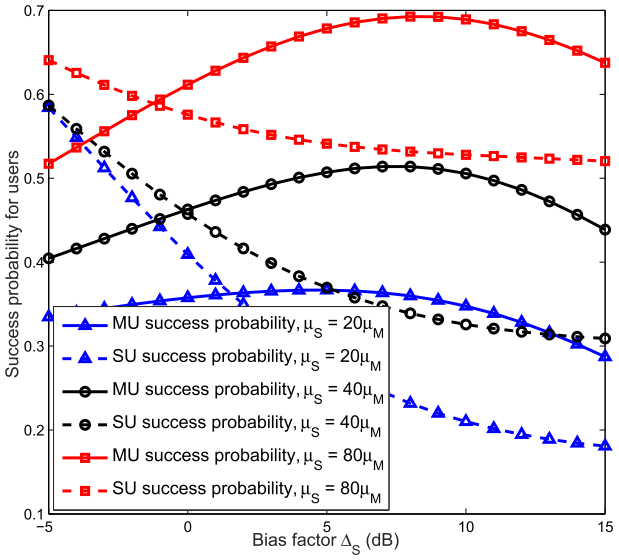

FIGURE 3. Per tier user success probability versus bias factor Δ_S for different SC densities with $\varepsilon = 4$dB.

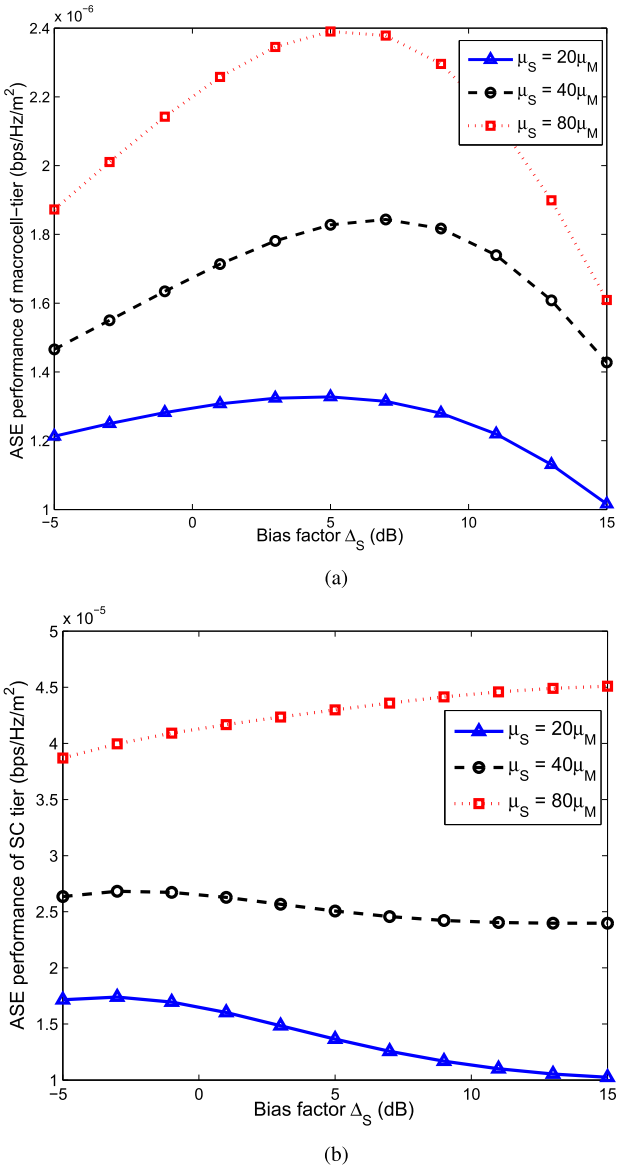

FIGURE 4. ASEs of macrocell and SC tiers versus bias factor Δ_S with $\varepsilon = 4$dB. (a) ASE of macrocell tier. (b) ASE of SC tier.

area increases. On the other hand, the MU success probability increases initially with the bias factor in the small bias factor region, reaches a maximum value depending on the SC density, and decreases from thereon. It is because of the aggregate effect of co-tier interference from other MUs and cross-tier interference from SUs. For small bias factor Δ_S, the macrocell coverage is large because more users are associated to MBSs. The larger coverage brings forth higher transmit power under the power control policy in (2) resulting in larger inter-cell interference that causes lower SINR. As the bias factor increases, the coverage of macrocells is decreased. Thus, the propagation distances between MUs and their serving MBS become shorter so that the transmit powers can be lowered resulting in less inter-cell interference and higher received SINR. As the bias factor increases further, the cross-tier interference stemming from the SC tier becomes much larger because the SU transmit power significantly increases according to the largely increased coverage.Furthermore, the higher the SC density, the higher are the SU and MU success probabilities. The reason for SUs is due to the increased SU association and the CTIA by using the coordinated subchannel allocation. For MUs, the reason is that the MUs are closer to MBSs and their received SINRs are likely above the threshold under the condition of higher SC density.

B. THE IMPACT OF BIAS FACTOR

Figures 4(a) and 4(b) plot the impact of bias factor Δ_S on the ASE performance for the macrocell tier and SC tier, respectively. According to (6), the curves in the two figures are the product of the corresponding curves in Figs. 2 and 3 times $\log_2(1+\epsilon)$. In Fig. 4(a), it is shown that the behavior of the ASE of the macrocell tier is similar to that of the MU success probability. It is because the equivalent active MU density is almost constant for different bias factors. In Fig. 4(b), it is shown that the ASE performance is improved as the bias factor increases for high SC density. However, when the SC density is low, the ASE performance is smaller in the low and high bias factor regions. The reason is that the increasing rate of the equivalent active SU density is higher than that of the SU success probability for high SC density, while it is vice versa for small SC density in the large bias factor region. Comparing the ASE of the two tiers, the ASE of the SC tier is dominating and higher than that of the macrocell tier especially for large SC density. It shows that the proposed biased cell association with the coordinated interference avoidance is effective to increase the ASE of SCs.

Figure 5 plots the system ASE versus bias factor Δ_S for different SC densities. The system ASE is the sum of the ASE

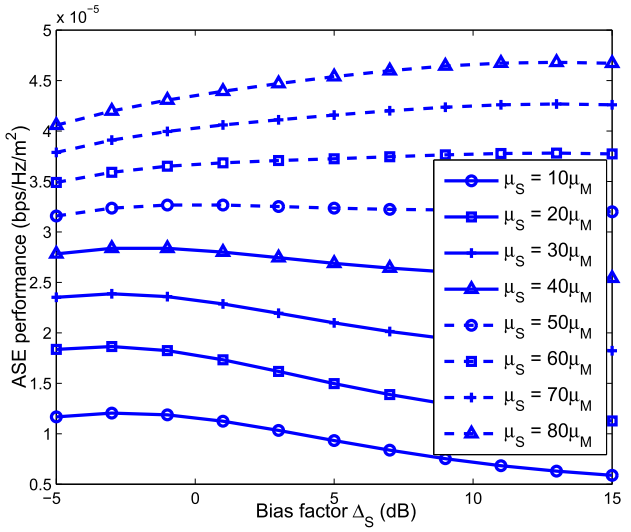

FIGURE 5. ASE performance versus bias factor Δ_S for different SC densities with $\varepsilon = 4$dB.

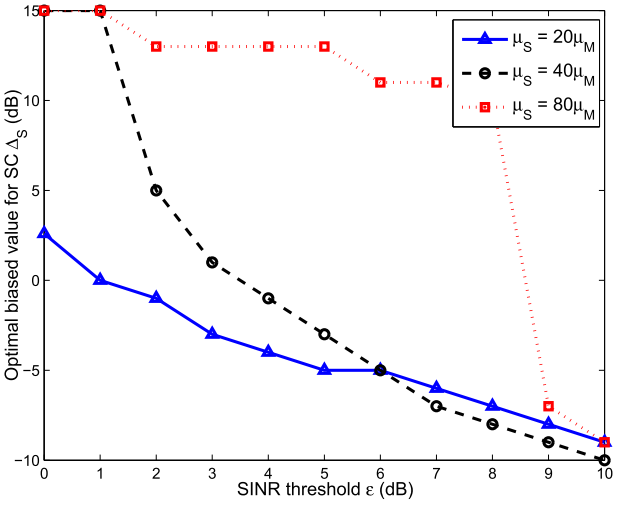

FIGURE 6. Optimal bias factor versus SINR threshold ε with $\mu_S = [20\mu_M, 40\mu_M, 80\mu_M]$, and $\Delta_{\max} = 15$dB.

of the macrocell and SC tiers. It is shown that the system ASE behavior follows closely to that of the SC tier, for example, the larger the SC density, the larger is the system ASE. It is because the ASE of the SC tier is dominating. In the figure, it can be observed that for a fixed SINR threshold, the optimal bias factor for the peak ASE is dependent on the SC density.

C. OPTIMAL BIAS FACTOR

The optimal bias factor can be obtained as

$$\Delta_S^\star = \underset{\Delta_S \le \Delta_{\max}}{\operatorname{argmax}} \, \mathrm{ASE}, \tag{46}$$

where $\Delta_{\max}$ is the maximum bias factor determined by the processing capacity of SBSs. The optimal bias factor is obtained via the bisection method with initial bias factor interval $[-10\text{dB}, 15\text{dB}]$.

Figure 6 plots the optimal bias factor in (46) obtained via the bisection method versus SINR threshold for different SC densities. The results show that the optimal bias factor is decreased as the SINR threshold ε increases. It means that for larger ε, the scheme is to reduce the SC association resulting in reduced SC coverage. It is because the proposed biased association scheme chooses to shrink the SC coverage that results in reducing the propagation distances between SUs and their serving SBSs and achieving the target SINR threshold. In doing so, more subchannels can be reserved for CTIA. Furthermore, the co-tier interference power caused by the interfering SUs is reduced because the SU transmit power is lowered in accordance with the propagation distance from SUs to their serving SBS. As a result, the success probability of SUs derived in (30) and (31) in Subsection III-D are improved. From Figs. 4-6, it can be observed that the proposed scheme for multichannel HCNs results in a large range of the optimal bias factors (depending on the system setups, e.g., density and SINR threshold), which is different from the corresponding result in [21] for which the minimum path loss association without interference avoidance is always optimal w.r.t. ASE for full-load HCNs. It reflects that the proposed scheme is able to make an effective tradeoff between increasing subchannel usage efficiency and reducing cross-tier interference.

D. SUBCHANNEL OCCUPIED PROBABILITY

Figure 7 plots the occupied probability per SC subchannel versus SINR threshold ε for biased and unbiased association schemes. The occupied probability is computed by (12). The usefulness of incorporating the CTIA into the biased association scheme is evaluated. It is shown that the occupied probability of using the proposed biased association scheme keeps constant for small ε because of the maximum bias constraint. The occupied probability is decreased as ε keeps increasing for the biased association scheme with (w/) or without (w/o) the CTIA because the optimal bias factor is decreased as ε increases leading to fewer SUs per SC. Furthermore, the occupied probability of the proposed biased association with the CTIA scheme is always less than that without the CTIA. The reason is that the proposed scheme needs to reserve more subchannels for interference avoidance. Besides, the occupied probability for the biased association scheme is larger than that of the unbiased one for small ε, and it is vice versa for large ε. It is because the biased association scheme can expand or shrink the coverage area of SCs with the optimal bias factor.

E. OPTIMAL ASE PERFORMANCE

Figure 8 plots the ASE performance versus SC density with $\varepsilon = 0$, 4dB for different association schemes. The association schemes, namely, the proposed optimal bias scheme with and without the CTIA, unbiased association with and without the CTIA, and the optimal uplink association scheme in [21], are compared in the figure. It is shown that the theoretical analysis is agreeable with the simulation results. The ASE is increased as the SC density increases because more users are

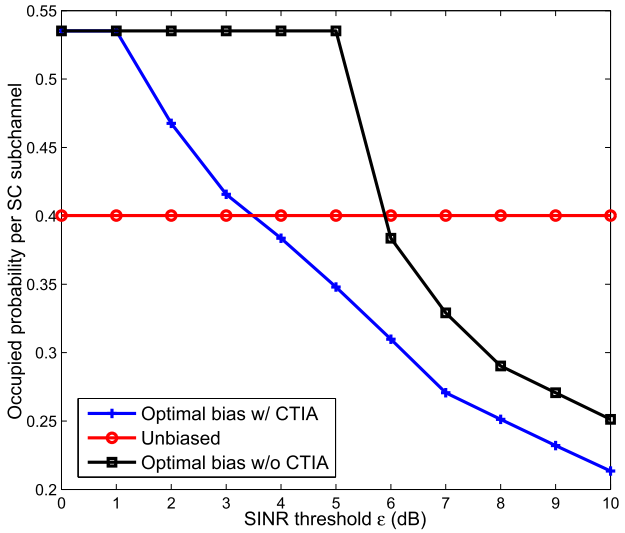

FIGURE 7. Occupied probability per SC subchannel versus ε with $\mu_S = 40\mu_M$, and $\Delta_{\max} = 15$dB.

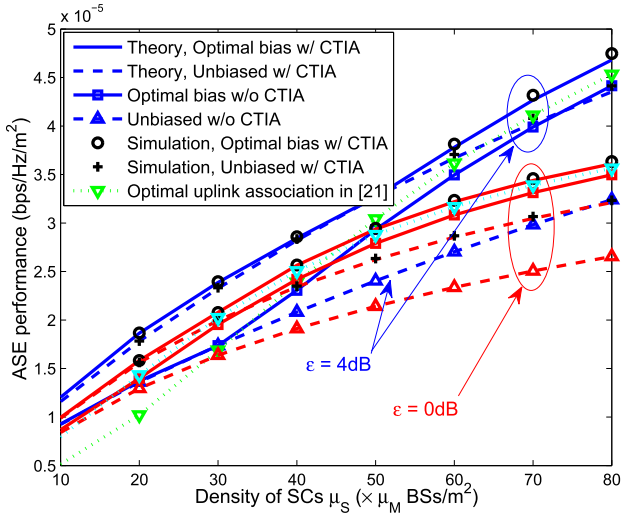

FIGURE 8. ASE performance versus SC density μ_S with $\Delta_{\max} = 15$dB.

offloaded to SCs. It is shown again that the SCs are effective to enhance spectral efficiency. In the figure, we notice that the ASE performance of the optimal bias scheme with the CTIA is close to that of the unbiased one for low SC density. It is because at the low SC density, the optimal bias factor of the proposed scheme is close to zero. As the SC density increases, the performance gap between the biased association scheme and the unbiased one becomes larger. Furthermore, the proposed biased association with the CTIA is superior to the existing scheme w.r.t. the ASE, especially for low SC density and higher SINR threshold. The reason is that more practical components and interference coordination are taken into account in the proposed scheme. This indicates the importance of incorporating both CTIA and biased association in the SC deployment of multichannel HCNs.

Figure 9 plots the ASE performance versus received SINR threshold with SC density $\mu_S = 20\mu_M, 80\mu_M$ for the

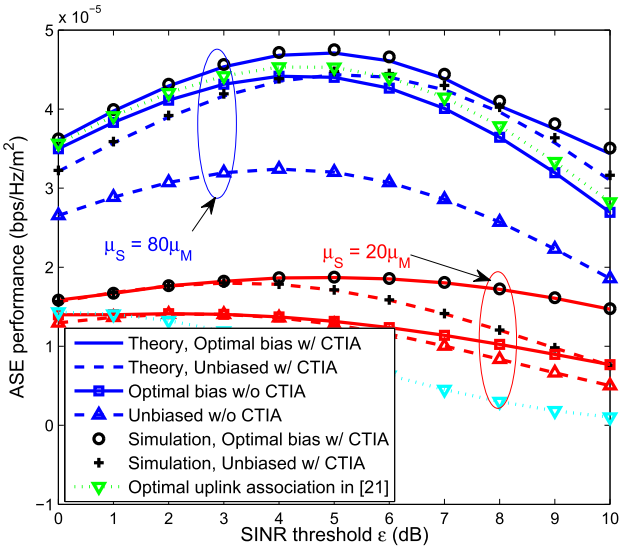

FIGURE 9. ASE performance versus SINR threshold ε for different SC densities with $\Delta_{\max} = 15$dB.

different association schemes used for Fig. 8. It is shown that the theoretical analysis agrees with the simulation results very well. For small SINR threshold, the ASE is increased as ε increases. The optimal ε for the peak ASE are different for the five association schemes. When ε is larger than the peak SINR threshold (depending on the SC density), the ASE decreases with ε. The explanation is given as follows. The ASE is determined by the aggregate effect of success probability and transmission rate as given in (6). When the SINR threshold ε increases, the transmission rate is increased, whereas the success probabilities derived in (32) and (33) are decreased because of the limitation of maximum transmit power and interference. When ε is large, the effect of success probability is more dominant on the ASE performance. As a result, the ASE is decreased in the large ε region. Besides, at certain SINR thresholds, the ASE values for the bias scheme and unbiased one are very close. It is because the optimal biases for these SINR thresholds are close to zero, as shown in Fig. 6. For $\mu_S = 20\mu_M$, there is an intersection point of the ASE curves of the biased and unbiased association schemes. The reason is that the optimal bias is zero for that SINR threshold. Furthermore, the ASE performance of the proposed scheme is superior to that of the optimal scheme in [21], and the performance gap increases with the SINR threshold ε.

In both Figs. 8 and 9, the proposed bias scheme with the CTIA is able to outperform upon other schemes that do not take interference avoidance or biased association into consideration. The performance gain depends on the SC density and SINR threshold ε.

V. CONCLUSIONS

In this paper, the ASE performance analysis of the proposed biased association scheme with the coordinated subchannel

allocation for multichannel HCNs is presented. The theoretical analysis is verified by simulation and agrees with the simulation results well. It is shown that the proposed scheme has the ability to adjust the bias factor according to the SC density and SINR threshold to maximize the ASE. The ASE analysis is expressed in a compact form to facilitate the optimization of the bias factor numerically. The proposed biased association scheme with interference avoidance can significantly improve the ASE in HCNs and its ASE performance is shown to be superior to that of the existing biased association scheme without the interference avoidance.

REFERENCES

[1] N. Bhushan *et al.*, "Network densification: The dominant theme for wireless evolution into 5G," *IEEE Commun. Mag.*, vol. 52, no. 2, pp. 82–89, Feb. 2014.
[2] S. Guo, C. Xing, H. Wang, Z. Pan, and Z. Fei, "Distributed optimization for downlink broadband small cell networks," in *Proc. IEEE Int. Conf. Commun.*, Jun. 2015, pp. 3472–3476.
[3] H. Wang, S.-H. Leung, and R. Song, "Analysis of uplink ICI and IBI in heterogeneous cellular networks with multiple macrocells," *IEEE Commun. Lett.*, vol. 21, no. 1, pp. 212–215, Jan. 2017.
[4] H. Du *et al.*, "A load fairness aware cell association for centralized heterogeneous networks," in *Proc. IEEE Int. Conf. Commun.*, Jun. 2015, pp. 2178–2183.
[5] A. Anpalagan, M. Bennis, and R. Vannithanby, *Design and Deployment of Small Cell Networks*. Cambridge, U.K.: Cambridge Univ. Press, 2016.
[6] F. Baccelli and B. Blaszczyszyn, *Stochastic Geometry and Wireless Networks*. Breda, The Netherlands: Now, 2010.
[7] H. Hu, H. Wang, Q. Zhu, and Z. Pan, "Uplink performance analysis in multi-tier heterogeneous celluar networks with power control and biased user association," *China Commun.*, vol. 13, no. 12, pp. 25–36, Dec. 2016.
[8] S. Mukherjee, *Analytical Modeling of Heterogeneous Cellular Networks Geometry, Coverage, and Capacity*. Cambrige, U.K.: Cambrige Univ. Press, 2014.
[9] J. G. Andrews, H. Claussen, M. Dohler, S. Rangan, and M. C. Reed, "Femtocells: Past, present, and future," *IEEE J. Sel. Areas Commun.*, vol. 30, no. 3, pp. 497–508, Apr. 2012.
[10] V. Garcia, Y. Zhou, and J. Shi, "Coordinated multipoint transmission in dense cellular networks with user-centric adaptive clustering," *IEEE Trans. Wireless Commun.*, vol. 13, no. 8, pp. 4297–4308, Aug. 2014.
[11] H. S. Dhillon, R. K. Ganti, F. Baccelli, and J. G. Andrews, "Modeling and analysis of K-tier downlink heterogeneous cellular networks," *IEEE J. Sel. Areas Commun.*, vol. 30, no. 3, pp. 550–560, Apr. 2012.
[12] W. C. Cheung, T. Q. S. Quek, and M. Kountouris, "Throughput optimization, spectrum allocation, and access control in two-tier femtocell networks," *IEEE J. Sel. Areas Commun.*, vol. 30, no. 3, pp. 561–574, Apr. 2012.
[13] S.-M. Cheng, W. C. Ao, F.-M. Tseng, and K.-C. Chen, "Design and analysis of downlink spectrum sharing in two-tier cognitive femto networks," *IEEE Trans. Veh. Technol.*, vol. 61, no. 5, pp. 2194–2207, Jun. 2012.
[14] V. Naghshin, M. C. Reed, S. V. Hanly, and N. Aboutorab, "Downlink coverage analysis of two-tier heterogeneous networks with asynchronous slots," in *Proc. IEEE Int. Conf. Commun.*, May 2016, pp. 1–6.
[15] H. Wang, R. Song, and S.-H. Leung, "Optimal uplink access in cognitive femtocell networks with adaptive modulation," *IEEE Commun. Lett.*, vol. 20, no. 5, pp. 1050–1053, May 2016.
[16] *Evolved Universal Terrestrial Radio Access (E-UTRA); Physical Layer Procedures, Rev. V9.1.0*, document TS 36.213, LTE, 2010.
[17] V. Chandrasekhar and J. G. Andrews, "Uplink capacity and interference avoidance for two-tier femtocell networks," *IEEE Trans. Wireless Commun.*, vol. 8, no. 7, pp. 3498–3509, Jul. 2009.
[18] H. ElSawy and E. Hossain, "On stochastic geometry modeling of cellular uplink transmission with truncated channel inversion power control," *IEEE Trans. Wireless Commun.*, vol. 13, no. 8, pp. 4454–4469, Aug. 2014.
[19] J. Acharya, L. Gao, and S. Gaur, *Heterogeneous Network in LTE Advanced*. Hoboken, NJ, USA: Wiley, 2014.
[20] A. Damnjanovic *et al.*, "A survey on 3GPP heterogeneous networks," *IEEE Wireless Commun.*, vol. 18, no. 3, pp. 10–21, Jun. 2011.
[21] S. Singh, X. Zhang, and J. G. Andrews, "Joint rate and SINR coverage analysis for decoupled uplink-downlink biased cell association in HetNets," *IEEE Trans. Wireless Commun.*, vol. 14, no. 10, pp. 5360–5573, Oct. 2015.
[22] T. Zahir, K. Arshad, A. Nakata, and K. Moessner, "Interference management in femtocells," *IEEE Commun. Surveys Tuts.*, vol. 15, no. 1, pp. 293–311, 1st Quart., 2013.
[23] N. Chakchouk and B. Hamdaoui, "Uplink performance characterization and analysis of two-tier femtocell networks," *IEEE Trans. Veh. Technol.*, vol. 62, no. 9, pp. 4057–4068, Nov. 2012.
[24] J. G. Andrews, F. Baccelli, and R. K. Ganti, "A tractable approach to coverage and rate in cellular networks," *IEEE Trans. Commun.*, vol. 59, no. 11, pp. 3122–3134, Nov. 2011.
[25] Y. Dhungana and C. Tellambura, "Performance analysis of SDMA with inter-tier interference nulling in HetNets," *IEEE Trans. Wireless Commun.*, vol. 16, no. 4, pp. 2153–2167, Apr. 2017.
[26] S. M. Yu and S.-L. Kim, "Downlink capacity and base station density in cellular networks," in *Proc. IEEE Int. Symp. Model. Mobile, Ad Hoc WiOpt Netw.*, May 2013, pp. 119–124.
[27] Y. Dhungana and C. Tellambura, "Multichannel analysis of cell range expansion and resource partitioning in two-tier heterogeneous cellular networks," *IEEE Trans. Wireless Commun.*, vol. 15, no. 3, pp. 2394–2406, Mar. 2016.
[28] M. Bacha, Y. Wu, and B. Clerckx, "Downlink and uplink decoupling in two-tier heterogeneous networks with multi-antenna base stations," *IEEE Trans. Wireless Commun.*, vol. 16, no. 5, pp. 2760–2775, May 2017.
[29] T. D. Novlan, H. S. Dhillon, and J. G. Andrews, "Analytical modeling of uplink cellular networks," *IEEE Trans. Wireless Commun.*, vol. 12, no. 6, pp. 2669–2679, Jun. 2013.
[30] K. Smiljkovikj, P. Popovski, and L. Gavrilovska, "Analysis of the decoupled access for downlink and uplink in wireless heterogeneous networks," *IEEE Wireless Commun. Lett.*, vol. 4, no. 2, pp. 173–176, Apr. 2015.
[31] H. ElSawy, A. Sultan-Salem, M. S. Alouini, and M. Z. Win, "Modeling and analysis of cellular networks using stochastic geometry: A tutorial," *IEEE Commun. Surveys Tuts.*, vol. 19, no. 1, pp. 167–203, 1st Quart., 2017.
[32] S. N. Chiu, D. Stoyan, W. S. Kendall, and J. Mecke, *Stochastic Geometry and Its Applications*, 3rd ed. Hoboken, NJ, USA: Wiley, 2013.
[33] M. Haenggi, *Stochastic Geometry for Wireless Networks*. Cambridge, U.K.: Cambridge Univ. Press, 2013.
[34] I. S. Gradshteyn and I. M. Ryzhik, *Table of Intergrals, Series and Products*, 7th ed. San Diego, CA, USA: Academic, 2007.

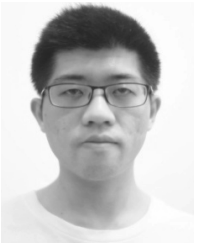

HONG WANG received the B.S. degree in telecommunications engineering from Jiangsu University, Zhenjiang, China, in 2011, and the Ph.D. degree from the Department of Telecommunications Engineering, Nanjing University of Posts and Telecommunications, Nanjing, China, in 2016.

From 2014 to 2015, he was a Research Assistant with the Department of Electronic Engineering, City University of Hong Kong, Hong Kong. From 2016 to 2018, he was a Senior Research Associate with the State Key Laboratory of Millimeter Waves, Department of Electronic Engineering, City University of Hong Kong. Since 2016, he has been an Instructor with the Department of Telecommunication Engineering, NUPT. His research interests include broadband wireless communications, particularly in interference analysis and management in HetNets.

SHU-HUNG LEUNG received the B.Sc. degree (Hons.) in electronics from The Chinese University of Hong Kong, Hong Kong, in 1978, and the M.Sc. and Ph.D. degrees in electrical engineering from the University of California at Irvine in 1979 and 1982, respectively.

From 1982 to 1987, he was an Assistant Professor with the University of Colorado at Boulder. Since 1987, he has been with the Department of Electronic Engineering, City University of Hong Kong, Hong Kong, where he is currently an Associate Professor. He has received a number of grants from the Competitive Earmarked Research Grant, the Croucher Foundation, and the CityU Strategic Grant. He has published over 200 technical papers in journals and international conference proceedings. His current research interests include MIMO communications and cooperative communications in heterogeneous networks.

Dr. Leung served as the Chairman of the Signal Processing Chapter of the IEEE Hong Kong Section in 2004 and as an organizing committee member for a number of international conferences. He is listed in Marquis Who's Who in Science and Engineering and Marquis Who's Who in the World. He is currently an Associate Editor of the IEEE TRANSACTIONS ON VEHICULAR TECHNOLOGY.

RONGFANG SONG received the B.S. and M.S. degrees from the Nanjing University of Posts and Telecommunications (NUPT), Nanjing, China, in 1984 and 1989, respectively, and the Ph.D. degree from Southeast University, Nanjing, in 2001, all in telecommunications engineering.

From 2002 to 2003, he was a Research Associate with the Department of Electronic Engineering, City University of Hong Kong, Hong Kong. Since 2002, he has been a Professor with the Department of Telecommunications Engineering, NUPT. His research interests include broadband wireless communications, with current focus on network multiple-input-multiple-output, interference management in HetNets, and compressed sensing-based signal processing.